Biochimica et Biophysica Acta, 686 (1982) 99–109
Elsevier Biomedical Press

BBA 71078

AUTO-OXIDATION-INDUCED FUSION OF LIPID VESICLES

KLAUS GAST [a], DIETRICH ZIRWER [a], AXEL-MICHAEL LADHOFF [b], JOACHIM SCHREIBER [c], REGINE KOELSCH [d], KONRAD KRETSCHMER [d] and JÜRGEN LASCH [d]

[a] Central Institute of Molecular Biology of the Academy of Sciences of the G.D.R., 1115 Berlin, Lindenberger Weg 70 (G.D.R.), [b] Department of Electron Microscopy of the Pathological Institute of the Humboldt University, Berlin (G.D.R.), [c] Central Institute of Isotope and Radiation Research, 1115 Berlin, Lindenberger Weg 70 (G.D.R.) and [d] Institute of Physiological Chemistry of the Martin Luther University, Halle (Saale) (G.D.R.)

(Received July 21st, 1981)
(Revised manuscript received October 28th, 1981)

Key words: Lipid auto-oxidation; Membrane stability; Liposome fusion

Spontaneous size changes of small unilamellar vesicles with initial mean diameters of 25 nm measured by quasi-elastic light scattering (QELS) and electron microscopy are reported. After the size conversion the vesicles have mean diameters of about 70 nm and are of the unilamellar and multilamellar type. The fact that auto-oxidation initiates this process is established by the comparison of the results for vesicles which differ only in the degree of auto-oxidation. The role of phosphatidylcholine hydroperoxides as fusogens is discussed.

Introduction

In the last decade phospholipid multibilayer and monobilayer vesicles have been intensively studied as models of biological membrane structure and function [1] and as potential drug delivery devices [2].

The small liposomes produced by the removal of detergent from mixed micelles of phospholipids and cholate [3] have often been employed for physical studies because of their narrow size distribution and their unilamellar structure as well as for biochemical studies because of the relative ease with which integral membrane proteins can be incorporated into this type of model membrane [4]. However, apart from the fact that the bilayer of these vesicles differs in certain respect from that of the less curved large multilamellar liposomes and biological membranes, time-dependent transformations of small vesicles into larger structures were observed under a variety of conditions. Spontaneous changes in the size distribution of dipalmitoyl- and distearoylphosphatidylcholine vesicles below, but not above, the phase transition temperature were reported by Schullery et al. [5] and Larrabee [6]. On the other hand, sonicated phosphatidylcholine vesicles have been found to be stable in size only below the transition temperature [7] or unstable under all conditions [8]. With dimyristoylphosphatidylcholine vesicles a size change occurs only in the phase transition region and appears to require a fusogen such as free fatty acid [9]. Van Dijck et al. [10] have observed a behaviour which is consistent with the conversion of small vesicles to large structures during the course of repeated calorimetric scans. Part of this disagreement may represent real differences in the vesicle system, particularly contamination by trace amounts of fusogens such as bivalent cations known to induce fusion of charged phospholipids [11,12] or free fatty acids.

Whether small vesicles of pure phosphati-

Abbreviation: QELS, quasi-elastic light scattering.

dylcholines are stable below, above or at the phase transition temperature has not been unambiguously established, nor has the nature of the particles to which the vesicles are converted or the mechanism of the conversion. Proposed mechanisms include vesicle-vesicle fusion [13,10,5], aggregation [14], rupture of vesicles [12] and transfer of phospholipid molecules [13,15,16]. In some instances the size of structures to which the small vesicles are converted have been found to be remarkably homogeneous and stable. So, small sonicated vesicles (diameter approx. 30 nm) were converted to larger vesicles by incubation below the phase transition temperature. The resulting most stable vesicle population had a diameter of 60–70 nm [5,6] and was claimed to be unilamellar vesicles. However, the proof of the unilamellar nature of transformed vesicles is traditionally beset with many difficulties arising from the limitations of the techniques of detection and from artifacts.

Our studies revealed another factor responsible for an increase in size of egg phosphatidylcholine small liposomes above the transition temperature, which might account for some of the conflicting results obtained with saturated and unsaturated phospholipid vesicles. We provide evidence that auto-oxidation of unsaturated alkyl chains of phosphatidylcholine molecules induces an increase in vesicle size. In other words, trace amounts of hydroperoxide derivatives of the fatty acid components of phospholipid act as fusogens.

It is well known that the presence of oxygen during the preparation of lipid vesicles affects the barrier properties of the lipid bilayer [17]. In the present work a correlation is established between the degree of auto-oxidation which is measured by the ultraviolet absorption at 233 nm [17,18] and the size changes of small unilamellar egg phosphatidylcholine liposomes during 'aging'. On the basis of electron microscopic studies we attribute the observed size increase to a fusion process.

Materials and Methods

Preparation and characterization of small unilamellar liposomes

Egg yolk phosphatidylcholine was purified according to Singleton et al. [19]. The product obtained by this procedure showed a single component on thin-layer chromatography identical with synthetic phosphatidylcholine. The chloroform/methanol solution (9:1, v/v) containing about 20 mg of phosphatidylcholine per ml was stored in sealed glass ampoules at −20°C and used within 2 months. Liposomes were prepared by the method of Brunner et al. [3]. Briefly, 2 ml of phosphatidylcholine stock solution were dried in a homogenizer under a stream of nitrogen, and a film of phosphatidylcholine was formed on the vessel wall. The dry lipid film was homogenized with 3 ml of sodium carbonate buffer, pH 8.0, containing 0.1 mol KCl per liter and 1.3% (w/v) of sodium cholate. The mixed phospholipid-cholate micelles were then allowed to equilibrate overnight at 4°C. The equilibrated mixture was passed over a Sephadex G-75 column (1.5 × 20 cm) to remove the detergent. The sample buffer without cholate served as elution buffer. The lipid-containing fractions were united, concentrated by vacuum dialysis with an immersible CX molecular separator (Millipore, U.S.A.) and rechromatographed on a Sepharose 4-B column (1.5 × 30 cm). The lipid concentrations of the fractions were determined as inorganic phosphorus by the method of Ames [20]. Only fractions containing particles of an average diameter of about 30 nm as judged by analytical gel chromatography on Sepharose 4B * according to Ackers [21] were used for further measurements.

'Oxidized and 'non-oxidized' vesicles were produced by small variations in the preparation procedure. In order to prepare 'oxidized' liposomes, the phosphatidylcholine film on the homogenizer wall was formed under a stream of analytical grade nitrogen (approx. 10 vol. % of oxygen) whereas in the preparation procedure for 'non-oxidized' liposomes the nitrogen was bubbled through an alkaline solution of pyrogallol and then dried over $CaCl_2$.

'Non-oxidized' vesicles were used as a reference sample. All fractions of vesicles employed in further experiments were additionally controlled with respect to their size and size homogeneity by analytical ultracentrifugation. To this end sedimenta-

* Calibration was done with thyroglobulin, rat liver ribosomes, and the plant virus Erysimum latent having Stokes' radii of 8, 11.8 and 15 nm, respectively.

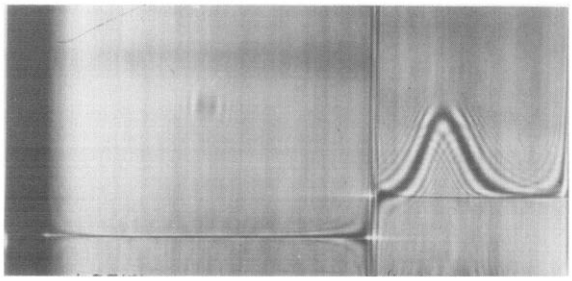

Fig. 1. Sedimentation pattern of small liposomes. $c = 4.2$ mg phosphatidylcholine/ml; buffer, KCl-$NaHCO_3$ buffer, 0.1 mol/l each, 20°C; sedimentation time, 68 min; $\omega = 4712\ s^{-1}$ (45000 rev./min), phase-plate angle = 10° (80°), solvent density = 1.0088 g/cm^3, $s_{20} = 2.32 \cdot 10^{-13}$ S (±1.5%), double-sector cell with an optical path of 12 mm.

tion coefficients and the symmetry of the Schlieren peak of the liposomes were determined in the Phywe ultracentrifuge U60L (Fig. 1). The gradient curves were divided by a line perpendicular to the base line passing the maximum of the Schlieren peak. The quotient of the two areas under the gradient curve constructed in this way served as a measure of symmetry. Only vesicles with this quotient in the range 1.00 ± 0.05 were used for further studies.

Quasi-elastic light scattering (QELS)

Quasi-elastic light scattering spectroscopy is a technique which measures the temporal fluctuations in the intensity of light scattered from a dispersion of particles (lipid vesicles in the present work). The analysis of the time dependence of the detected light of randomly fluctuating intensity in terms of the frequency spectrum or the autocorrelation function yields the translational diffusion coefficient of the particles. In liposome dispersions such fluctuations are almost completely due to changes in the local positions of these particles (liposomes) caused by the translational diffusion. A number of excellent reviews on the theory and data analysis of this technique are available in the literature [22–24].

In our studies the apparatus described in Ref. 25 was employed. In addition to the He-Ne laser HNA 188, an argon laser ILA-120 operating at $\lambda = 488$ nm and 100 mW output power was used (both lasers are manufactured by VEB Carl Zeiss Jena, G.D.R.). The measurements were done in the homodyne autocorrelation mode with the help of the 100-point correlator NSA-1000 (EMG, Hungary). The data were stored on paper tape for further data processing on a process computer KRS 4200 (Robotron, G.D.R.).

The square root of the measured correlation function was either fitted by the sum of two exponentials or analyzed by the cumulant method [26,27]. The angular variations of the light scattering intensities and the correlation times were measured mostly using the argon laser while for the measurements over longer periods of time the He-Ne laser was preferred. All samples were cleaned by filtering the vesicle suspensions through 0.2 μm Nuclepore filters directly into the rectangular scattering cells. The cells were stored at temperatures between 20 and 23°C during the whole time of observation. QELS and integrated intensity measurements were carried out with one and the same optical arrangement.

The degree of oxidation was monitored by a spectroscopic method described in Ref. 17 measuring the ultraviolet absorption at 233 nm. The ratio of the absorbances A_{233}/A_{215} is only a rough quantitative estimate for the degree of oxidation. A volume of 0.1 ml of the vesicle suspension was dissolved in 3 ml ethanol. The measurements were done in a Beckman Acta C V spectrophotometer. The term 'oxidized' means here that only the higher unsaturated fatty acid residues are oxidized, exactly speaking the phosphatidylcholines of these samples are 'partly oxidized' or 'preoxidized'.

Electron microscopy

Electron microscopy was carried out by placing a drop of the vesicle suspension at room temperature on a carbon-coated cellulose nitrate supporting film. After an adsorption time of 3 min the suspension was removed by filter paper and negative staining was done in wet state by a 2% aqueous solution of ammonium molybdate, pH 7.1. Grids were air-dried and viewed with a Siemens 102 electron microscope operating at 80 kV. Primary magnification was 80000. Vesicle size measurements were done from micrographs with a MOP-digitizer (Kontron, F.R.G.). More than 1000 vesicles were sized for each distribution.

Results

QELS and ultraviolet absorption

The temporal behaviour and the phenomenon of fusion of the vesicles were studied by QELS on a number of samples divided in two groups with the notation A for 'oxidized' and B for 'non-oxidized' lipid vesicles, respectively. The suspensions of group A showed a pronounced ultraviolet absorption in the range of 233 nm as a result of the formation of conjugated dienes [17,18] in comparison to suspensions of group B.

As an example of stable vesicles we discuss sample B1. In connection with this discussion it is necessary to make some general remarks regarding the interpretation of the QELS results from all vesicle suspensions investigated in this study. The corrected relative scattering intensities as a function of the scattering angle θ are shown in Fig. 2. Vesicles with sizes of the order of 20–30 nm (approx. $\lambda/20$) cannot produce such a strong dependence of the light scattering intensity on θ because their particle scattering function $P(\theta)$ is nearly equal to one for all θ at $\lambda = 488$ nm. At $\theta = 15°$, the smallest scattering angle used in this work, the intensity of light scattered from a sample cell containing the buffer is only 0.1% of the scattering intensity of sample B1 immediately after filtration (The contribution of the light scattering background is of the same order for all samples investigated and can be disregarded in any case.). The increase in light scattering at small angles is therefore an inherent feature of the vesicle suspensions and must be attributed to the presence of trace amounts of larger particles. The amount of these large aggregates of lipid material increases if the suspensions are stored for several days at room temperature, but it is only of the order of 1% of the weight concentration. Although this is of minor importance for the bulk suspension it considerably complicates QELS and integrated light scattering measurements, especially at small scattering angles (see Figs. 2 and 4). If a suspension contains particles of different sizes, two fundamental schemes of data evaluation exist. Provided the number of discrete sizes is small, the correlation function can be fitted by a sum of exponentials, each representing one of these discrete sizes having a radius R_i and a diffusion coefficient D_i. If the number of sizes is large (in practice > 3) and/or these sizes are not very different or there is a continuous distribution of sizes, the method of cumulants [26,27] is suitable to give mean values of R and D and parameters characterizing the width and the skewness of the size distribution.

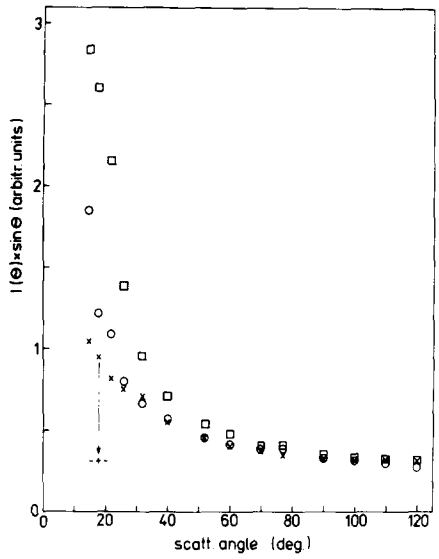

Fig. 2. Angular dependence of the integrated light scattering intensity of sample B1 at various times: ×, immediately; ○, one day and □, 6 days after filtration. $\lambda = 488$ nm, $t = 20°C$. -+-, the contribution of vesicles calculated from the results of Table I.

Because lipid vesicles have such a continuous size distribution around a mean value, the cumulant analysis should be the method of choice. Determining the first two cumulants $K_1 = \bar{\Gamma}$ and $K_2 = \overline{\Gamma^2} - \bar{\Gamma}^2$ one is able to calculate the z-averaged diffusion coefficient

$$\langle D \rangle = \bar{\Gamma} q^{-2} = K_1 q^{-2} \tag{1}$$

and its relative variance

$$\sigma^2 = \left(\langle D^2 \rangle - \langle D \rangle^2\right) / \langle D \rangle^2 = K_2 / K_1^2 \tag{2}$$

where the angular brackets denote a z-average, and q is the scattering vector

$$q = \frac{4\pi}{\lambda} \sin(\theta/2) \tag{3}$$

(λ, wavelength in the scattering medium; θ, scattering angle). The diffusion coefficient D is related to the hydrodynamic Stokes' radius by the Stokes-Einstein relation

$$R_s^{-1} = \frac{6\pi\eta}{kT} D \qquad (4)$$

(k, Boltzmann constant; T, absolute temperature; η, solvent viscosity). In the case of polydisperse samples a z-average of R_s^{-1} is obtained for $q \to 0$. We shall use the notation

$$R_{app} = \langle R_s^{-1} \rangle^{-1} \qquad (5)$$

to characterize the apparent vesicle radius.

However, the presence of distinct large particles in vesicle suspensions not only leads to unrealistically large values of K_2 and σ^2 but also enhances the measured apparent diameter $2R_{app}$ considerably (this behaviour is demonstrated in Table III). Under these circumstances the only way to get reasonable results is to fit the correlation function $g^{(1)}(\tau)$ by a sum of two exponentials

$$g^{(1)}(\tau) = A_1 \exp(-\Gamma_1\tau) + A_2 \exp(-\Gamma_2\tau) \qquad (6)$$

where the A_i are functions of the ith particle mass, concentration and particle scattering function. The Γ_i are related to discrete size classes $2R_i$ as $\bar{\Gamma}$ to the apparent mean values (Eqns. 1 and 4). $i = 1$ stands for the vesicles and $i = 2$ for the aggregates. Note that this is only an approximation to eliminate the contribution of the large aggregates to the correlation function. The remaining component $2R_1$ is then a better estimate of the average vesicle size and should agree with the results of the cumulant method in cases where the contribution of large aggregates can be neglected. Approximating the correlation function by the sum of two exponentials no further conclusions can be drawn about the width of the distribution of vesicle sizes around $2R_1$. Fortunately, the situation is more favorable in the case of vesicles of group A, especially after the change in vesicle size, so that the cumulant analysis can be used at large scattering vectors. The results of a bimodal fit for sample B1 immediately after filtration are given in Table I for small and large scattering vectors. Besides the vesicles with diameters of the order of 25 to 30 nm

TABLE I

RESULTS OF A BIMODAL FIT TO THE AUTOCORRELATION FUNCTIONS OF SAMPLE B1

$\lambda = 488$ nm; $t = 20°C$; $c = 1.5$ mg·ml^{-1}.

θ (°)	q^2 (cm^{-2}) ($\times 10^{-10}$)	$2R_1$ (nm)	$2R_2$ (nm)	A_2/A_1
18	0.288	29.7	400	2.0
90	5.89	26.4	720	0.17
90 *	5.89	28.1	440	0.29

* Measured after 6 days.

aggregates with sizes around 400 nm can be detected. The ratio of the amplitudes A_2/A_1 is also a measure of the contribution of both particle classes to the total light scattering intensity. The contribution from vesicles at a scattering angle $\theta = 18°$ is shown in Fig. 2. The results of the measurement after 6 days show that the only effect is an increased number of aggregates while the size of the vesicles and their contribution to light scattering at large scattering angles remains constant.

In contrast to this behaviour, vesicles of group A undergo a remarkable change in size reflected in changes of the correlation functions and the scattering intensities at large scattering angles. Some features of this conversion process for a number of samples are summarized in Table II. The influence of the concentration on this process can only be considered for vesicles of the same preparation, because only these have the same 'history'. The size conversion is discussed in more detail in connection with samples A1 and A2.

The increase in size for sample A1 at two concentrations is demonstrated in Fig. 3. The time $t = 0$ corresponds to the beginning of the experiment when the sample was brought to room temperature and filtered into the scattering cells. The time when fusion begins and the rate constant of this process are strongly dependent on lipid concentration. The average vesicle size reaches a new, well defined, mean value which shows only a little decrease at longer times.

The dependence of the inverse reduced scattering intensity on the square of the scattering vector q is shown in Fig. 4. The influence of the large aggregates can be seen at small q^2. After fusion

TABLE II

SUMMARIZED DATA CHARACTERIZING THE FUSION PROCESS OF VARIOUS SAMPLES

D_i, D_f initial and final diffusion coefficients; $(2R_{app})_i$, $(2R_{app})_f$ initial and final diameters; I_f/I_i increase in scattering intensity; t_{con} approximate time of size conversion (defined by the time interval between 10% and 90% of the total size increase). C_{pc}, concentration of phosphatidylcholine.

Sample	C_{pc} ($mg \cdot ml^{-1}$)	$D_i^{20,w}$ ($cm^2 \cdot s^{-1}$) ($\times 10^7$)	$D_f^{20,w}$ ($cm^2 \cdot s^{-1}$) ($\times 10^7$)	$2R_{app,i}$ (nm)	$2R_{app,f}$ (nm)	I_f/I_i	t_{con} (h)
A1a	4.5	1.74±0.14	0.61±0.03	24.5±2.0	70.5±3.0	6.5	12
A1b	2.3	1.74±0.14	0.55±0.03	24.5±2.0	77.5±3.5	9.6	33
A2	2.8	1.38±0.13	0.63±0.03	31.0±3.0	67.5±3.0	4.2	7
A3a	4.6	1.75±0.14	0.55±0.03	24.4±2.0	77.4±3.5	9.9	9
A3b	1.5	1.76±0.18	0.54±0.03	24.3±2.5	79.0±4.0	14.8	70
A4	1.8	1.68±0.15	0.53±0.03	25.4±2.3	81.2±4.0	9.7	–

the average vesicle size is large enough so that the slope of c/I versus q^2 for $q^2 > 2 \cdot 10^{10}\ cm^{-2}$ (where the contribution of aggregates is negligible) can be used to determine the z-average of the radius of gyration, which is (32 ± 3) nm and (37 ± 4) nm for A1a and A1b, respectively. The fusion process at lower concentrations is slower but the final average vesicle size is larger, as can be deduced from the radius of gyration as well as from the apparent diameter from QELS experiments. In Table III we present the QELS results of sample A1a before

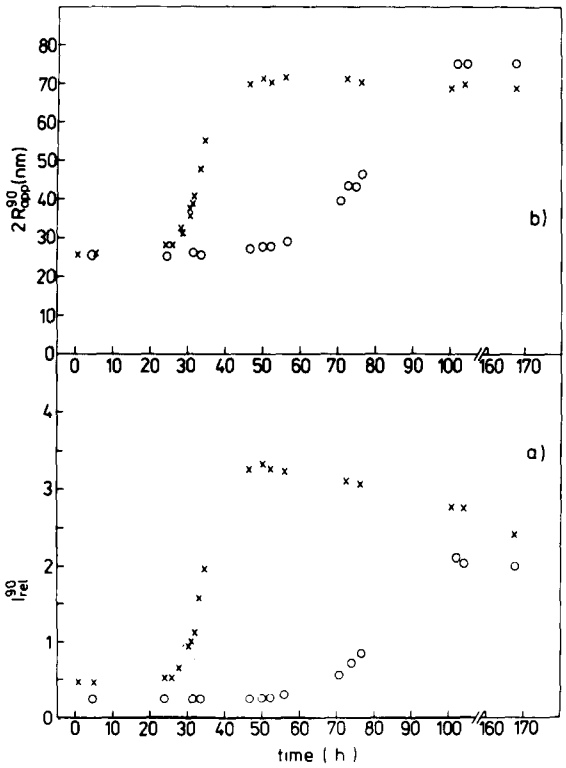

Fig. 3. Time dependence of (a) the scattering intensity and (b) the apparent diameters measured at a scattering angle 90° and wavelength λ=633 nm on samples A1a (×) and A1b (○).

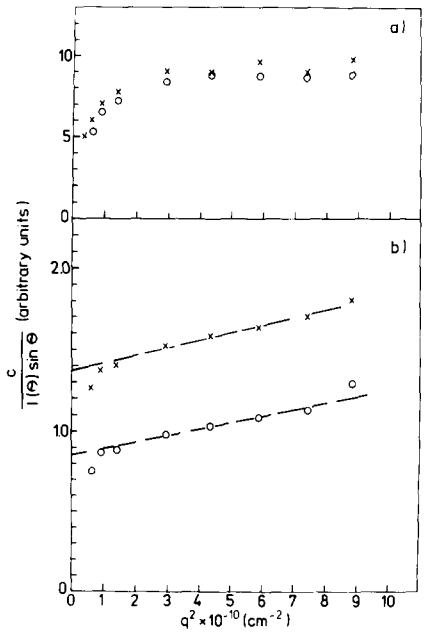

Fig. 4. Inverse reduced relative scattering intensities (a) before and (b) after fusion of sample A1a (×) and A1b (○). The slopes in Fig. 4b give radii of gyration of (31.7±3.0) nm and (37.4±4.0) nm for A1a and A1b, respectively.

TABLE III

APPARENT DIAMETERS $2R_{app}$ FOR A UNIMODAL SIZE DISTRIBUTION AND DIAMETERS $2R_1$ FOR A BIMODAL DISTRIBUTION FOR SAMPLE A1a

$\lambda = 488$ nm; $t = 20°C$.

q^2 (cm^{-2}) ($\times 10^{-10}$)	$2R_{app}$ (nm)	$2R_1$ (nm)	$2R_2$ (nm)	A_2/A_1
0.335	43.5	24.8	380	0.75
0.596	37.1	22.9	400	0.56
1.38	29.6	25.6	370	0.18
2.95	27.7	23.2	400	0.14
5.89	25.6	–	–	–
8.84	24.9	–	–	–

fusion at various scattering vectors. $2R_{app}$, calculated from the first cumulant, is remarkably enhanced at small scattering angles due to the presence of aggregates. At small angles we must take the component $2R_1$ of the bimodal fit as a measure of the vesicle size. These values and $2R_{app}$ of the cumulant method at large angles are used to define the apparent initial diameter given in Table II. As in the case of the sample B1 the size of the aggregates is of the order of 400 nm. Apparent diameters before and after vesicle fusion of sample A1a are shown in Fig. 5. In the case of fused vesicles the cumulant method gives reasonable results over a large range of q^2 so that an extrapolation to $q^2 = 0$ is possible (excluding only the smallest q^2). For particles which are large enough to exhibit an angular-dependent scattering function $P(\theta)$ z-averages can only be calculated for $q^2 = 0$. The slope of $2R_{app}$ versus q^2 is produced by the polydispersity of the vesicles. In principle, this slope can be used to characterize the size inhomogeneity [28], but in our case it is still too weak for quantitative estimates. To characterize the polydispersity, we have calculated the second cumulant (Eqn. 2). From this we found a value $\sigma^2 = 0.09 \pm 0.03$ for the fused vesicles at $\theta = 90°$ and $\lambda = 488$ nm. Under certain circumstances $2R_{app}$ and σ^2 can be used to determine also the width of the number distribution of sizes and other number averaged quantities. But for these calculations one must assume a particular distribution function and a defined relation between the mass and the radius of the particles. This is not well established in our case.

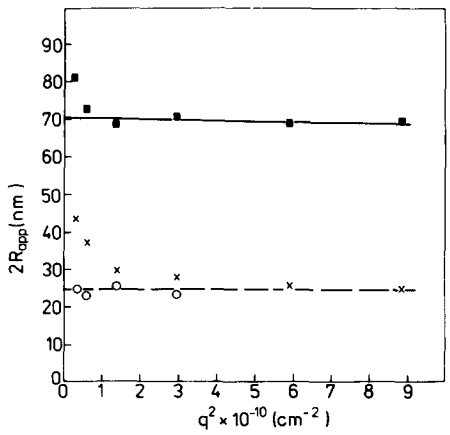

Fig. 5. Apparent diameter for a unimodal size distribution (×) and the component $2R_1$ (○) for a bimodal distribution before fusion of sample A1a, (■) apparent diameters for a unimodal size distribution after fusion of sample A1a.

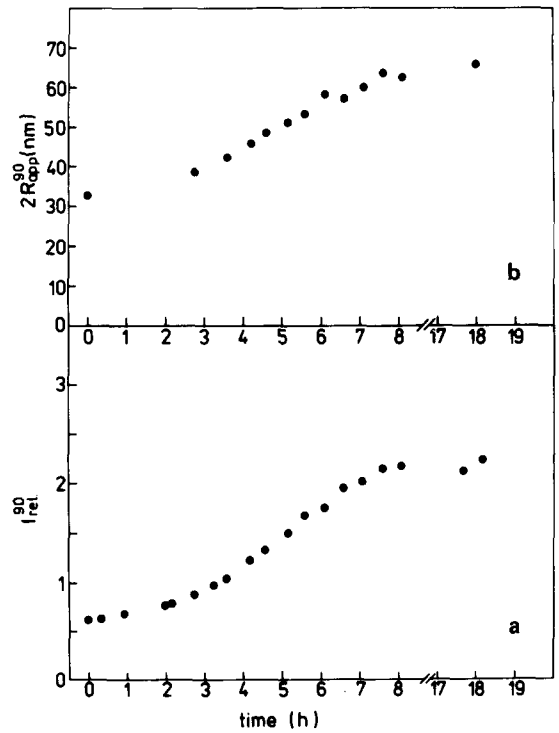

Fig. 6. Time dependence of (a) the integrated scattering intensity and (b) the apparent diameters measured at a scattering angle 90° and wavelength $\lambda = 633$ nm on sample A2.

TABLE IV

APPARENT DIAMETERS CALCULATED FROM THE HISTOGRAMS OF FIGS. 8a AND 8b.

	Calculated apparent diameter (nm)	
	from Fig. 8a	from Fig. 8b
Single bilayer	50	77
Multibilayer	69	75

The change in the average size of the vesicles of sample A2 is demonstrated in Fig. 6. Although this sample behaves similar to sample A1, the results are shown because electron micrographs have been taken in parallel with these QELS experiments. The increases in average vesicle size as well as in scattering intensity are smaller than in the case of sample A1.

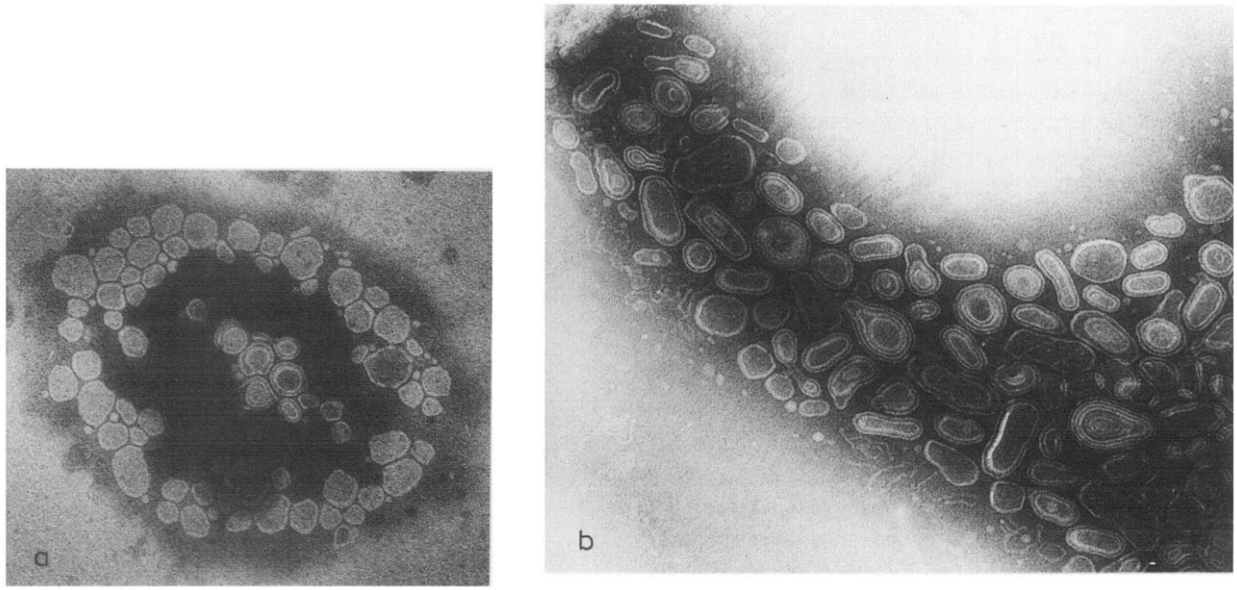

Fig. 7. Electron micrographs of vesicles of sample A2 taken (a) immediately after the filtration of the sample (at zero time, Fig. 6) and (b) after one day. The total magnification is 100000.

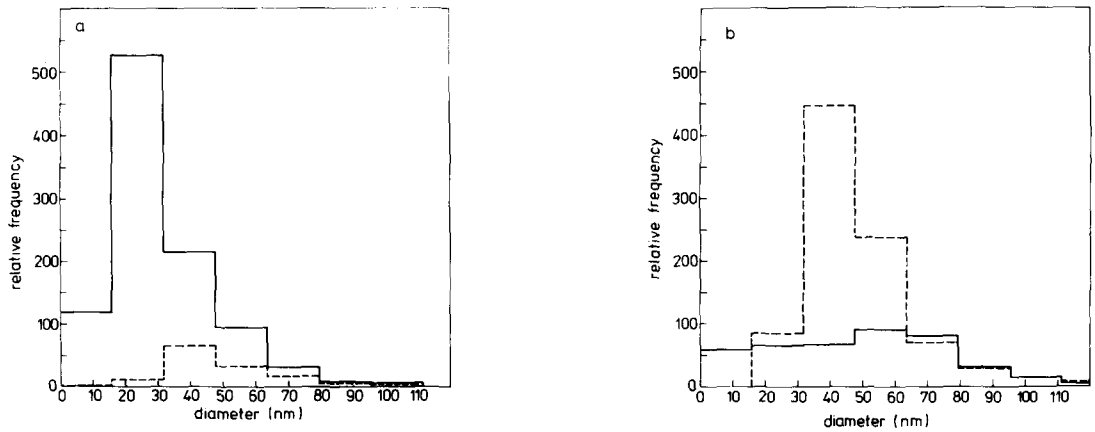

Fig. 8. Size distributions determined from electron micrographs of vesicles of sample A2 (a) before and (b) after fusion. The total number of sized particles was 1130 for (a) and 1313 for (b). ————, single bilayer vesicles; ------, multi bilayer vesicles.

Electron microscopy

The electron micrographs of vesicles taken at the time of the beginning of the QELS experiments on sample A2 and after one day are shown in Figs. 7a and 7b, respectively. The corresponding histograms are plotted in Figs. 8a and 8b. The conversion of single bilayer vesicles to larger single bilayer and multibilayer vesicles is clearly demonstrated.

Discussion

Both methods, electron microscopy and QELS, clearly indicate the change in vesicle size, but each has its problems in characterizing this process. Electron microscopy can answer the question as to what kind of particles the single bilayer vesicles are converted. With more than 1000 vesicles sized, the most frequent diameters are fairly well established and representative of the whole dispersion. Only in the tails of the histograms the number of sized vesicles is too small for a good statistics. One problem which exists with electron microscopy, especially in this case, is that the system is not in an equilibrium state and the concentration plays an important role. Therefore influences of the airdrying procedure and the adsorption on the grid cannot be excluded. In other words, whether the small multilamellar liposomes seen in Fig. 7 were already present in the vesicle dispersion or are the result of the airdrying procedure cannot be decided unequivocally, though there are some indications from the scattering experiments that the primary fusion products are large unilamellar vesicles. This conclusion could be drawn comparing the increase of the scattering intensity, which is proportional to the increase of the mass of the vesicles with the increase of the Stokes' radii of the vesicles. But these considerations are complicated due to the size inhomogeneity of the vesicles. Comparing the sizes measured by both methods one must take into account that the diameters derived from QELS are z-averages and may be shifted considerably to larger values in comparison to the number-averaged diameters evaluated from the histograms if we have a broad size distribution. For a comparison we must therefore calculate the z-averaged radii for the number distribution in the histograms. To exclude the low scattering angle range, we calculated a z-average which is modified by the scattering function $P(\theta) \equiv P(qR)$

$$\langle R^{-1} \rangle = \frac{\int_0^\infty P(qR)\, g(R)\, M^2(R)\, R^{-1}\, \mathrm{d}R}{\int_0^\infty P(qR)\, g(R)\, M^2(R)\, \mathrm{d}R} \tag{7}$$

where M is the vesicle mass. The integral can be replaced by the sum of the contributions of the different size classes, assuming the product of the number density of particles $g(R)$ and the scattering function to be constant:

$$P(qR)\, g(R)/_{R_{i-1}}^{R_i} = P(q\bar{R}_i)\, \frac{N_i}{\Delta R} \tag{8}$$

$\Delta R = R_i - R_{i-1}$ is the ith size range, N_i the number of particles and R_i the mean radius of the ith size class. The problem in these computations is that there is no unique and simple relation between the mass and the radius of the vesicles of the various types. We used $M^2(R) = \text{const. x } R^m$ with the limits $4 \leq m \leq 6$ for hollow and compact spheres, respectively. Eq. (7) then takes the form

$$\langle R^{-1} \rangle = \frac{(m+1) \sum_{i=1}^{S} N_i P(q\bar{R}_i)\, (R_i^m - R_{i-1}^m)}{m \sum_{i=1}^{S} N_i P(q\bar{R}_i)\, (R_i^{m+1} - R_{i-1}^{m+1})} \tag{9}$$

S is the total number of size classes.

As an approximation we used $m = 4$ for single bilayer, $m = 5$ for multibilayer vesicles, and the scattering function $P(qR) = (\sin qR/qR)^2$ for hollow spheres. The calculations were carried out separately for single and multi-bilayer vesicles for $\theta = 90°$ and $\lambda = 488$ nm. From the histogram before fusion we get apparent diameters of 50 nm and 69 nm and from the histogram after fusion diameters of 77 nm and 75 nm for single bilayer and multibilayer vesicles, respectively. After fusion the agreement with the experimental data from quasi-elastic light scattering (sample A2, Fig. 6) is rather good. The poor agreement before fusion may have the following reasons. Because QELS is very sensitive to large particles the experimental

values can be considered as upper limits. Therefore it is reasonable to assume that the size histogram of Fig. 8a reflects a transient state at the beginning of the fusion process which may be induced by the preparation of the sample for electron microscopy.

A remarkable feature of the fusion process in samples of type A is that a stable final equilibrium state is reached in contrast to the formation of unspecific large aggregates demonstrated by the results of sample B1. A detailed interpretation of this size conversion is complicated by the fact that large single bilayer vesicles as well as small and large multibilayer vesicles are formed.

Diffusion of single molecules from one vesicle to another or flocculation or aggregation of the vesicles can be ruled out on the basis of the reported experimental results. Therefore the observed size change is interpreted as a fusion process. But with its relative slowness, with its induction period, and with the observed multilayered structures it is a more complicated process than, e.g., the intensively investigated Ca^{2+}-induced fusion of phosphatidylserine [29] or phosphatidic acid [30] containing negatively charged vesicles. In these cases there is no comparable induction period before fusion. The half-time for fusion lies in the range from 1 to 10 min [30]. The spontaneous fusion of dipalmitoylphosphatidylcholine vesicles yields large, closed unilamellar vesicles [5].

The concentration dependence of the time constant of the vesicle conversion can be explained by the increased probability of encounter of two vesicles as the concentration increases. To bring about a 3-fold increase in vesicle size, at least about ten small vesicles must undergo fusion. We ascribe the time lag of the onset of the conversion process at lower concentrations (cf. Fig. 3) to an enhanced fusion ability of the fusion products of two or three vesicles.

As the basic reason for the complexity of the auto-oxidation driven process of size variation we have to mention that egg phosphatidylcholine is a mixture of phosphatidylcholine (PC) molecules with various fatty acids of different reaction rates and also different reaction products during auto-oxidation [18].

In the following we try to consider the observed size change with respect to the general steps of fusion known from the literature [31]. The first condition of the fusion of cells or vesicles, i.e. a sufficiently extended area of uncovered lipid bilayer (no electrostatic or steric hindrance of the apposition of two bilayers), is fulfilled in our experiments.

The encounter of two vesicles leads, in a first step, to a close juxtaposition of the two bilayers. This fast step is reversible if pure phospholipids without any trace amounts of fusogenic compounds are employed (reversible aggregation). If, on the other hand, fusogenic agents are present, a second step, the formation of non-bilayer structures in the contact region, is triggered. The existence of non-bilayer structures (hexagonal packing, reversed micelles) between two monolayers, called 'lipidic particles', is now well established [32,33]. Such non-bilayer structures are adopted by amphiphilic molecules whose molecular shape is cone-like in contrast to the more rod-like shape of phosphatidylcholines [34]. Moreover, these structures are favored by calcium ions bridging head groups of charged lipid molecules.

A condition for fusion to occur is, that the contact area of colliding vesicles contains a sufficiently large number of such amphiphiles for which the lamellar phase is an energetically unfavorable state. In small vesicles these molecules tend to assume an energetically favored state by special orientations, mainly by segregation into clusters or domains, resulting in local disturbances of the vesicle surface as indicated for instance by enhanced permeability. When two such vesicles come into close contact the fusion-inducing molecules relax into the above mentioned non-bilayer structures. The contact layer is destabilized and the rearrangement of the molecules (third step) entails fusion.

Auto-oxidation of liposomes produces by radical chain reactions relatively stable phosphatidylcholine hydroperoxides which have not a rod-like molecular geometry. In the case of linoleate residues for instance the bulky, polar-OOH groups are situated at position 9 or 13 [35] within the hydrophobic part of the bilayer. The oxidised lipid molecules are not randomly distributed within the bilayer and enhance the permeability [36]. We suggest, therefore, that the phosphatidylcholine hydroperoxides form non-bilayer structures when

the vesicles come into close contact. The observd correlation between the induction period before the onset of vesicle size changes and before the formation of measurable amounts of lipid hydroperoxides supports this suggestion.

Another explanation cannot be ruled out, however, namely that other products of the autooxidation process such as cyclic peroxides, epoxides, polymerised or broken phosphatidylcholine molecules are active fusogens [37].

References

1 Capaldi, R.A. (1977) Membrane Proteins, Vol. 1: Membrane Proteins and their Interactions with Lipids, Marcel Dekker, Inc., New York and Basel
2 Gregoriadis, G. (1973) FEBS Lett. 36, 292–296
3 Brunner, J., Skrabal, P. and Hauser, H. (1976) Biochim. Biophys. Acta 455, 322–331
4 Hall, E.R. and Brodbeck, U. (1978) Eur. J. Biochem. 89, 159–167
5 Schullery, S.E., Schmidt, C.F., Felgner, P., Tillack, T.W. and Thompson, T.E. (1980) Biochemistry 19, 3919–3923
6 Larrabee, A.L. (1979) Biochemistry 18, 3321–3326
7 Tsong, T.Y. (1974) Proc. Natl. Acad. Sci. U.S.A. 71, 2684–2688
8 Sheetz, M. and Chan, S. (1972) Biochemistry 11, 4573–4581
9 Kantor, H.L. and Prestegard, J.H. (1978) Biochemistry 17, 3592–3597
10 Van Dijck, P.W.M., De Kruijff, B., Aarts, P.A.M.M., Verkleij, A.J. and De Gier, J. (1978) Biochim. Biophys. Acta 506, 183–191
11 Papahadjopoulos, D., Vail, W.J., Newton, C., Nir, S., Jacobson, K., Poste, G. and Lazo, R. (1977) Biochim. Biophys. Acta 465, 579–598
12 Ginsberg, L. (1978) Nature 275, 758–760
13 Lawaczeck, R., Kainosho, M. and Chan, S.I. (1976) Biochim. Biophys. Acta 443, 313–330
14 Petersen, N.O. and Chan, S.I. (1978) Biochim. Biophys. Acta 509, 111–128
15 Martin, F.J. and McDonald, R.C. (1976) Biochemistry 15, 321–327
16 Lawaczeck, R. (1978) J. Colloid Polym. Sci. 66, 247–256
17 Klein, R.A. (1970) Biochim. Biophys. Acta 210, 486–489
18 Schreiber, J. (1979) Pharmazie 34, 36–40
19 Singleton, W.S., Grey, M.S., Brown, M.L. and White, J.L. (1965) J. Am. Oil Chemists Soc. 42, 53
20 Ames, B.N. (1966) in Methods in Enzymology (Perlman, G.E. and Lorand, E., eds.), vol. 8, pp. 115–118
21 Ackers, G.K. (1967) J. Biol. Chem. 242, 3237–3238
22 Chu, B. (1974) Laser Light Scattering, Academic Press, New York
23 Cummins, H.Z. and Pike, E.R. (1974) Photon Correlation and Light Beating Spectroscopy, Plenum Press, New York
24 Berne, B.J. and Pecora, R. (1976) Dynamic Light Scattering, Wiley and Sons, New York
25 Gast, K., Zirwer, D., Fahrenbruch, B. and Pittelkow, R. (1979) Exp. Techn. Phys. 27, 319–329
26 Koppel, D. (1972) J. Chem. Phys. 57, 4814–4820
27 Brown, J.C., Pusey, P.N. and Dietz, R. (1975) J. Chem. Phys. 62, 1136–1144
28 Brehm, G.A. and Bloomfield, V.A. (1975) Macromolecules 8, 663–665
29 Sun, S.T., Hsang, C.C., Day, E.P. and Ho, J.T. (1979) Biochim. Biophys. Acta 557, 45–52
30 Liao, M.J. and Prestegard, J.H. (1980) Biochim. Biophys. Acta 599, 81–94
31 Cullis, P.R. and Hope, M.J. (1978) Nature 271, 672–674
32 Cullis, P.R. and De Kruijff, B. (1979) Biochim. Biophys. Acta 559, 399–420
33 De Kruijff, B., Cullis, P.R. and Verkleij, A.J. (1980) Trends Biochem. Sci. 5, 79–81
34 Wieslander, A., Christiansson, A., Rilfors, L. and Lindblom, G. (1980) Biochemistry 19, 3650–3655
35 Logani, M.K. and Davies, R.E. (1980) Lipids 15, 485–495
36 Mandal, T.K. and Chatterjee, S.N. (1980) Radiat. Res. 83, 290–302
37 Ahkong, Q.F., Fisher, D., Tampion, W. and Lucy, J.A. (1973) Biochem. J. 136, 147–152
38 Papahadjopoulos, D., Vail, W.J., Jacobson, K. and Poste, G. (1975) Biochim. Biophys. Acta 394, 483–491